

Comparison of UCA-OAM and UCA-MIMO Systems for Sub-THz Band Line-of-Sight Spatial Multiplexing Transmission

Gye-Tae Gil, Ju Yong Lee, Hoon Kim, and Dong-Ho Cho

Abstract: This paper compares the uniform circular array based orbital angular momentum (UCA-OAM) scheme, which enables spatial multiplexing transmission of data symbols via multiple OAM modes, with the UCA-MIMO scheme through numerical analysis and simulation in terms of spectral efficiency and feedback overhead. Specifically, based on the relations between the eigenmodes of the UCA-SVD-MIMO system and the modes of UCA-OAM system as well as the capacity formula, the channel capacities of the two systems are compared for the cases where equal power allocation and waterfilling power allocation are employed, and then the effectiveness of the analytical results are verified through simulation.

Index Terms: MIMO, orbital angular momentum, spatial multiplexing, uniform circular array.

I. INTRODUCTION

ORBITAL angular momentum (OAM) is one of the momentum of electromagnetic (EM) waves which is known to be conserved up to a far-field zone according to the momentum conservation law [1], [2]. As it was found that a theoretically infinite number of OAM modes, but practically finite, can be transferred without mutual interference in a line-of-sight (LoS) channel environment [3]–[8], there have been growing interests in this new technique in the fields of millimeter wave / sub-terahertz (sub-THz) and light beam communication [9]–[15].

The most important moments in the history of research on the radio OAM technique are as follows. In 2012, there was an experiment on wireless data transmission, in Panova univ., Italy, using a spiral phase plate (SPP) and a Yagi antenna, which proved the possibility of far-field transmission of radio OAM having a number of states [5]. In 2007, it was shown through simulation that a photonic OAM can be generated by the use of a uniform circular array (UCA) in the radio frequency range [6]. In 2010, it was found that a circular array antenna is sufficient for the generation of OAM modes, and that only local measure-

ments are necessary for the detection of the OAM modes [7]. Besides the UCA-based OAM, various techniques have been studied for the generation of electromagnetic OAM waves at radio frequency (RF) domain, including dielectric resonator antennas [16], traveling-wave cavity antennas [17], and metasurfaces [18]–[20].

Among the proposed systems, the OAM transmission system using a uniform circular array (UCA) with N antenna elements has the advantage that it constructs N parallel channels by employing the predetermined set of discrete Fourier transform (DFT) and inverse DFT on the transmitter and receiver sides [8]. A radio OAM system which employs a UCA, however, was faced with the question of whether it is the same as the existing multiple input multiple output (MIMO) transmission technique because the UCA is just a kind of array with multiple antenna elements [8]. Research is still needed to find a clear answer to this question.

In this paper, we compare the UCA-OAM scheme, which enables spatial multiplexing transmission of data symbols via multiple OAM modes, through numerical analysis and simulation in terms of spectral efficiency and feedback overhead with the UCA based singular value decomposition MIMO (UCA-SVD-MIMO) scheme.

To this end, the channel capacities of the two systems are compared for the cases where equal power allocation and waterfilling power allocation are employed, based on the channel capacity formula as well as the relation between the eigenmodes of the UCA-SVD-MIMO channel and the modes of the UCA-OAM channel. In addition, we demonstrate through numerical analysis that the UCA-OAM scheme can achieve the same spectral efficiency as the UCA-SVD-MIMO scheme with the exactly same feedback overhead, which means that the two systems are equivalent.

The remainder of the paper is organized as follows. Section II describes the system models of the UCA-OAM and UCA-SVD-MIMO schemes. Section III presents the analytical results. Section IV presents the numerical results. Section V contains the concluding remarks.

Contribution: The contribution of this paper lies in that the advantages of the UCA-OAM scheme over the UCA-SVD-MIMO scheme is justified for the first time taking feedback overhead into account. In addition, the relation between the mode gains of the UCA-OAM system and UCA-SVD-MIMO system is analyzed theoretically and verified through simulation.

Notations: \mathbf{A}^T , \mathbf{A}^H , $\text{tr}\{\mathbf{A}\}$, $\det(\mathbf{A})$, and $\mathbf{A}^{1/2}$ denote the transpose, the conjugate transpose, the trace, the determinant,

Manuscript received September 28, 2020; revised March 12, 2021; approved for publication by Ho-Jin Song, Guest Editor, March 24, 2021.

This work was supported by Institute for Information and Communication Technology Promotion (IITP) grant funded by the Korea government(MSIT) (No.2019-0-00826, High resolution intelligent Radcomm system).

G.-T. Gil and J. Y. Lee are with the KAIST Institute, Korea Advanced Institute of Science and Technology (KAIST), Korea, email: {gategil, jylee1117}@kaist.ac.kr.

H. Kim and D.-H. Cho are with School of Electrical Engineering, Korea Advanced Institute of Science and Technology (KAIST), Korea, email: {hoonkim, dhcho}@kaist.ac.kr.

G.-T. Gil is the corresponding author.

Digital Object Identifier: 10.23919/JCN.2021.000013

1229-2370/21/\$10.00 © 2021 KICS

Creative Commons Attribution-NonCommercial (CC BY-NC).

This is an Open Access article distributed under the terms of Creative Commons Attribution Non-Commercial License (<http://creativecommons.org/licenses/by-nc/3.0>) which permits unrestricted non-commercial use, distribution, and reproduction in any medium, provided that the original work is properly cited.

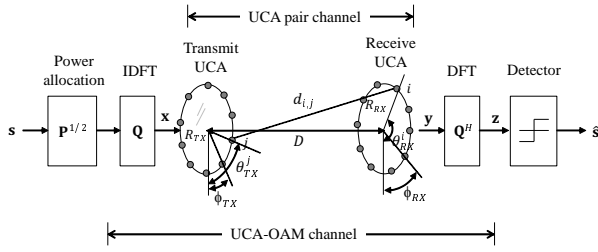


Fig. 1. UCA-OAM system model.

and the square-root operation of a matrix \mathbf{A} , respectively. $\text{Re}\{\cdot\}$ denotes the real part of the variable in the brackets. $|\mathbf{A}|$ denotes the matrix whose elements are equal to the magnitudes of the elements of \mathbf{A} .

II. SYSTEM MODEL

A. Generation of OAM with a UCA Antenna

The orbital angular momentum, L , of a sinusoidal electromagnetic wave generated by a UCA antenna is expressed as [7]

$$L = \varepsilon_0 \int \text{Re}\{\mathbf{i}\mathbf{E}^*(-\mathbf{i}(\mathbf{r} \times \nabla) \cdot \mathbf{A}_{UCA}(\mathbf{r}))\} dV, \quad (1)$$

where ε_0 is the vacuum permittivity, \mathbf{i} is the imaginary unit, and $\mathbf{A}_{UCA}(\mathbf{r})$ denotes the vector potential that appears at the position \mathbf{r} from the center of the UCA.

It was shown in [7] that if the phase of the current flowing into the n th antenna element becomes $2\pi ln/N$ where l is an integer, the vector potential at the position \mathbf{r} for a large N can be approximated as

$$\mathbf{A}_{UCA}(\mathbf{r}) \cong \mathbf{A}(\mathbf{r}) N \mathbf{i}^{-l} e^{il\varphi} J_l(ka \sin\theta), \quad (2)$$

where $\mathbf{A}(\mathbf{r})$ denotes the vector potential by a radiating antenna element of the UCA, φ is the azimuthal angle, θ is the elevation angle, k is the wave number (i.e., $k = 2\pi/\lambda$), a is the radius of the UCA, and $J_l(\cdot)$ is the l th order Bessel function of the first kind. This indicates that the sinusoidal EM wave generated by the UCA has momentum with azimuthal phase dependency, $e^{il\varphi}$ [7].

Accordingly, if a receive UCA is placed on a plane perpendicular to the propagation direction of the EM wave generated by the transmit UCA, the phase of the EM wave arriving at each element of the receive UCA becomes a rotating phase. Since the phases of different OAM modes of the EM wave are orthogonal on a circle of a plane perpendicular to the propagation direction, one can separate the desired mode l from the received signal by combining the phase shifter outputs following the receive UCA, where the phase shift for the n th UCA element is $-2\pi ln/N$.

The phase shifts for the transmit UCA element n , $2\pi ln/N$, can be generated by using a column of the inverse discrete Fourier transform (IDFT), and multiple sinusoidal EM waves can be superpositioned by using multiple columns of the IDFT matrix and then transmitted simultaneously.

B. UCA Pair Channel Model

Fig. 1 shows the system model for the UCA-OAM system considered in this paper. In this system, the transmit and receive

UCAs have radii of R_{TX} and R_{RX} , respectively, and the T-R distance between them is D . The antenna elements of both the transmit UCA and the receive UCA are arranged around a circle at equal intervals, and the angles of the transmitting element j and the receiving element i on the circle are $\theta_{TX}^j = 2\pi j/N + \phi_{TX}$ and $\theta_{RX}^i = 2\pi i/N + \phi_{RX}$, respectively.

In a pure LoS environment, the channel response between the transmit element j and the receive element i is expressed as

$$h_{i,j} = \beta \frac{\lambda}{4\pi d_{i,j}} \exp\left\{-\mathbf{i} \frac{2\pi d_{i,j}}{\lambda}\right\}. \quad (3)$$

Here, λ is the wavelength of the EM wave, β represents the gain and phase by the transmit and receive antennas, and $d_{i,j}$ is the distance between the two antenna elements which is given by

$$d_{i,j} = (D^2 + R_{TX}^2 + R_{RX}^2 - 2R_{TX}R_{RX}\cos\theta_{i,j})^{1/2}, \quad (4)$$

where

$$\theta_{i,j} = \theta_{RX}^i - \theta_{TX}^j = \frac{2(i-j)}{N} + \phi_{RX} - \phi_{TX}. \quad (5)$$

Note from (4) and (5) that $\theta_{i,j}$ is constant for all (i,j) pairs with an equal value of $i-j$, and so is $d_{i,j}$. This means that $h_{i,j}$ also has the same value for such pairs under the condition that β is a constant for a range of directions determined by the aperture of the receive UCA.

C. Signal Model for a UCA-OAM System

When the element-by-element channel $h_{i,j}$ is a constant for all (i,j) pairs with the same difference, the channel matrix of the UCA pair, $\mathbf{H} \in C^{N \times N}$, is said to be circulant, and this circulant matrix can be decomposed as a product of the IDFT matrix $\mathbf{Q} \in C^{N \times N}$, complex diagonal matrix $\mathbf{\Delta} \in C^{N \times N}$, and the DFT matrix $\mathbf{Q}^H \in C^{N \times N}$ as expressed by [8]

$$\mathbf{H} = \mathbf{Q}\mathbf{\Delta}\mathbf{Q}^H, \quad (6)$$

where the i th element in the diagonal entries of $\mathbf{\Delta}$ is denoted by a complex variable δ_i .

Hence, the signal vector $\mathbf{y} \in C^{N \times 1}$ that appears at the receive UCA can be written as

$$\mathbf{y} = \mathbf{H}\mathbf{x} + \mathbf{n} = \mathbf{Q}\mathbf{\Delta}\mathbf{Q}^H\mathbf{x} + \mathbf{n}, \quad (7)$$

where $\mathbf{n} \sim \mathcal{N}(0, \sigma_n^2 \mathbf{I}_N)$ is the additive white Gaussian noise (AWGN) and \mathbf{I}_N denotes the N -dimensional identity matrix. Suppose that the signal vector $\mathbf{x} \in C^{N \times 1}$ transmitted through the transmit UCA is written as

$$\mathbf{x} = \mathbf{Q}\mathbf{P}^{1/2}\mathbf{s}. \quad (8)$$

Then we have the DFT output $\mathbf{z} \in C^{N \times 1}$ as given by

$$\mathbf{z} = \mathbf{Q}^H\mathbf{y} = \mathbf{\Delta}\mathbf{P}^{1/2}\mathbf{s} + \mathbf{Q}^H\mathbf{n} \quad (9)$$

where $\mathbf{s} \in C^{N \times 1}$ is the data symbol and $\mathbf{P}^{1/2} \in C^{N \times N}$ is the power allocation matrix.

Since the matrix $\mathbf{\Delta}$ is diagonal, (9) indicates that N parallel channels can be constructed without the presence of mutual

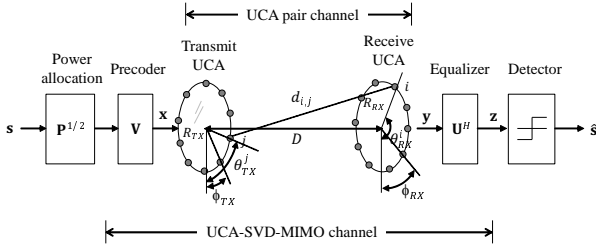


Fig. 2. System model for the UCA-SVD-MIMO scheme.

interference by transmitting and receiving the OAM EM wave by using the IDFT and DFT at the transmitter side and the receiver side, respectively. In this regard, the diagonal matrix Δ is referred to as the channel matrix of the UCA-OAM system.

Meanwhile, given the channel matrix \mathbf{H} , the average signal-to-noise ratio (SNR) appearing at the antenna elements of the receive UCA for $\mathbf{P} = \mathbf{I}_N$ is defined by

$$SNR = \frac{\|\mathbf{H}\|_F^2 \sigma_s^2}{N \sigma_n^2}, \quad (10)$$

where σ_s^2 is the average power of the data symbols in \mathbf{s} . Therefore, ρ defined as the ratio of the σ_s^2 to σ_n^2 can be calculated as

$$\rho = \frac{\sigma_s^2}{\sigma_n^2} = \frac{SNR}{\|\mathbf{H}\|_F^2 / N}. \quad (11)$$

In addition, since total transmit power P_t associated with the transmitted signal \mathbf{s} is equal to $N\sigma_s^2$, and P_t is also equal to the power in \mathbf{x} which is calculated as $E[\|\mathbf{x}\|^2] = \text{tr}\{\mathbf{P}\}\sigma_s^2$, we have

$$\text{tr}\{\mathbf{P}\} = \sum_{i=1}^N p_i = N. \quad (12)$$

D. Signal Model for a UCA-SVD-MIMO System

Fig. 2 shows the system model for the UCA-SVD-MIMO scheme. It is well known that the SVD based MIMO scheme can construct N parallel channels without mutual interference, and that it can achieve the maximum transmission capacity of the given MIMO channel by applying the waterfilling power allocation algorithm.

In a UCA-SVD-MIMO system, the given UCA pair channel \mathbf{H} can be decomposed as a product of a diagonal matrix Σ with N singular values as its diagonal elements, left singular matrix \mathbf{U} , and the right singular matrix \mathbf{V} , which is written by

$$\mathbf{H} = \mathbf{U}\Sigma\mathbf{V}^H, \quad (13)$$

where the k th element in the diagonal entries of Σ is denoted by a real variable σ_k .

Hence, the signal vector $\mathbf{y} \in C^{N \times 1}$ appearing at the receive UCA is written as

$$\mathbf{y} = \mathbf{H}\mathbf{x} + \mathbf{n} = \mathbf{U}\Sigma\mathbf{V}^H\mathbf{x} + \mathbf{n} \quad (14)$$

and when the signal transmitted through the transmit UCA is given by $\mathbf{x} = \mathbf{V}\mathbf{P}^{1/2}\mathbf{s}$, we have the equalizer output $\mathbf{z} \in C^{N \times 1}$ as given by

$$\mathbf{z} = \mathbf{U}^H\mathbf{y} = \Sigma\mathbf{P}^{1/2}\mathbf{s} + \mathbf{U}^H\mathbf{n} \quad (15)$$

which indicates that N parallel channels without mutual interference can be realized by transmitting the EM wave generated by using the right singular matrix \mathbf{V} and the left singular matrix \mathbf{U} at the transmitter side and the receiver side, respectively. In this regard, the diagonal matrix Σ is referred to as the channel matrix of the UCA-SVD-MIMO system.

III. ANALYTICAL RESULTS

In this section, the characteristics of the UCA-OAM system and the UCA-SVD-MIMO system are analyzed in terms of channel capacity and feedback overhead.

A. Channel Capacities with Equal Power Allocation

Assume that the noise appearing at the receive UCA is AWGN with zero-mean and covariance of $\sigma_n^2\mathbf{I}_N$, i.e., $\mathbf{n} \sim \mathcal{N}(0, \sigma_n^2\mathbf{I}_N)$. Then, when the equal power allocation is employed, it can be shown from (9) and (15) that the channel capacity corresponding to the UCA-OAM system and the UCA-SVD-MIMO system respectively can be written as

$$C_{\text{OAM}} = \log_2 \det(\mathbf{I}_N + \rho\Delta\Delta^H) \quad (16)$$

and

$$C_{\text{SVD-MIMO}} = \log_2 \det(\mathbf{I}_N + \rho\Sigma^2). \quad (17)$$

Under the equal power allocation, the channel capacities of two systems satisfy the relationship as described in Theorem 1.

Theorem 1: With equal power allocation, the capacity of the UCA OAM channel is exactly the same as that of the UCA-SVD-MIMO channel.

Proof: Since the square matrix \mathbf{Q} is unitary and (6) leads to $\Delta = \mathbf{Q}^H\mathbf{H}\mathbf{Q}$, (16) can be rewritten as

$$C_{\text{OAM}} = \log_2 \det(\mathbf{I}_N + \rho\mathbf{Q}^H\mathbf{H}\mathbf{Q}^H\mathbf{Q}\mathbf{H}^H\mathbf{Q}). \quad (18)$$

In addition, by using the unitary property of \mathbf{Q} and the property of $\det(\mathbf{A}\mathbf{B}) = \det(\mathbf{A})\det(\mathbf{B})$ for two square matrices \mathbf{A} and \mathbf{B} , (18) can be rewritten as

$$\begin{aligned} C_{\text{OAM}} &= \log_2 \det(\mathbf{I}_N + \rho\mathbf{Q}^H\mathbf{H}\mathbf{H}^H\mathbf{Q}) \\ &= \log_2 \det(\mathbf{Q}^H) \det(\mathbf{I}_N + \rho\mathbf{H}\mathbf{H}^H) \det(\mathbf{Q}) \\ &= \log_2 \det(\mathbf{I}_N + \rho\mathbf{H}\mathbf{H}^H). \end{aligned} \quad (19)$$

Likewise, since the matrices \mathbf{U} and \mathbf{V} are unitary, we get $\Sigma = \mathbf{U}^H\mathbf{H}\mathbf{V}$ from (13), and therefore (17) can be rewritten as

$$C_{\text{SVD-MIMO}} = \log_2 \det(\mathbf{I}_N + \rho\mathbf{U}^H\mathbf{H}\mathbf{V}\mathbf{V}^H\mathbf{H}^H\mathbf{U}). \quad (20)$$

In addition, by using the unitary property of \mathbf{U} and \mathbf{V} and the property of $\det(\mathbf{A}\mathbf{B}) = \det(\mathbf{A})\det(\mathbf{B})$ for two square matrices \mathbf{A} and \mathbf{B} , (20) can be rewritten as

$$\begin{aligned} C_{\text{SVD-MIMO}} &= \log_2 \det(\mathbf{I}_N + \rho\mathbf{U}^H\mathbf{H}\mathbf{H}^H\mathbf{U}) \\ &= \log_2 \det(\mathbf{U}^H) \det(\mathbf{I}_N + \rho\mathbf{H}\mathbf{H}^H) \det(\mathbf{U}) \\ &= \log_2 \det(\mathbf{I}_N + \rho\mathbf{H}\mathbf{H}^H). \end{aligned} \quad (21)$$

Based on (19) and (21), it is clear that both the UCA-OAM system and the UCA-SVD-MIMO system with equal power allocation have the same channel capacity. \square

B. Relation between OAM Mode Gains and Singular Values

From (16) and (17), the channel capacity of the UCA-OAM system and the UCA-SVD-MIMO system can be represented as a sum of mode capacities of N modes as follows:

$$C_{\text{OAM}} = \sum_{i=0}^{N-1} \log_2(1 + \rho |\delta_i|^2) \quad (22)$$

and

$$C_{\text{SVD-MIMO}} = \sum_{k=0}^{N-1} \log_2(1 + \rho \sigma_k^2), \quad (23)$$

where $|\delta_i|^2$ is the gain of the i th mode of the UCA-OAM channel and σ_k^2 represents the gain of the k th eigenmode of the UCA-SVD-MIMO channel. There is a relation between the term $|\delta_i|^2$ and σ_k^2 as described in Theorem 2.

Theorem 2: For a diagonal element σ_k^2 of Σ^2 , there exists a diagonal element $|\delta_i|^2$ of $\Delta\Delta^H$ corresponding to it with exactly the same value.

Proof: Using the SVD of $\mathbf{H} = \mathbf{U}\Sigma\mathbf{V}^H$ and the relation of $\Delta = \mathbf{Q}^H\mathbf{H}\mathbf{Q}$, it is straightforward to show that

$$\Delta\Delta^H = \mathbf{Q}^H\mathbf{U}\Sigma^2\mathbf{U}^H\mathbf{Q}, \quad (24)$$

which means that the singular value matrix of $\Delta\Delta^H$ is Σ^2 whose diagonal elements are sorted in decreasing order of magnitude. Define $\tilde{\Delta}$ as a diagonal matrix whose diagonal elements are the sorted version of the diagonal elements of Δ in decreasing order of magnitude. Then, it can be written that $\tilde{\Delta} = \mathbf{E}^T\Delta\mathbf{E}$ and $\Delta = \mathbf{E}\tilde{\Delta}\mathbf{E}^T$, where \mathbf{E} is a permutation matrix. Thus, we have

$$\Delta\Delta^H = \mathbf{E}\tilde{\Delta}\tilde{\Delta}^H\mathbf{E}^T, \quad (25)$$

which indicates that $\tilde{\Delta}\tilde{\Delta}^H$ is also the singular value matrix of $\Delta\Delta^H$.

From (24) and (25), both Σ^2 and $\tilde{\Delta}\tilde{\Delta}^H$ are the singular value matrix of $\Delta\Delta^H$, and this indicates that $\Sigma^2 = \tilde{\Delta}\tilde{\Delta}^H$ because the singular value matrix of a matrix is unique. Therefore, the diagonal entries of Σ^2 is a permuted version of the diagonal entries of $\Delta\Delta^H$, which means that for a diagonal element of Σ^2 , there is a diagonal element of $\Delta\Delta^H$ corresponding to it with exactly the same value. \square

C. Channel Capacities with Waterfilling Power Allocation

From (9) and (15), we have the channel capacity expressions for the UCA-OAM system and the UCA-SVD-MIMO system respectively given by

$$C_{\text{OAM}} = \log_2 \det(\mathbf{I}_N + \rho\mathbf{P}\Delta\Delta^H) \quad (26)$$

and

$$C_{\text{SVD-MIMO}} = \log_2 \det(\mathbf{I}_N + \rho\mathbf{P}\Sigma^2), \quad (27)$$

which can be rewritten as a sum of mode capacities as follows:

$$C_{\text{OAM}} = \sum_{i=0}^{N-1} \log_2(1 + \rho |\delta_i|^2 p_i) \quad (28)$$

and

$$C_{\text{SVD-MIMO}} = \sum_{k=0}^{N-1} \log_2(1 + \rho \sigma_k^2 p_k), \quad (29)$$

where p_i and p_k denote the i th and k th diagonal element of the power allocation matrix \mathbf{P} , and satisfy the total power constraint of $\sum_{i=1}^N p_i = N$ from (12).

From (28) and (29), it is clear that the achievable channel capacities of both the UCA-OAM system and the UCA-SVD-MIMO system can be maximized by waterfilling power allocation under total transmit power constraint, and they are equal to each other because, by Theorem 2, there always exists $|\delta_i|^2$ of the UCA-OAM channel corresponding to σ_k^2 of the UCA-SVD-MIMO channel.

D. Comparison in Terms of Feedback Overhead

In a perfectly aligned UCA pair system, the right singular matrix \mathbf{V} need not be fed back not only in a UCA-OAM system but also in a UCA-SVD-MIMO system. It is because the right singular matrix of \mathbf{H} which is required for SVD precoding is a column-wise permuted version of the IDFT matrix \mathbf{Q} as described in Theorem 3.

Theorem 3: The right singular matrix \mathbf{V} and the left singular matrix of \mathbf{H} are related to the IDFT matrix \mathbf{Q} as

$$\mathbf{V} = \mathbf{Q}\mathbf{S}_v\mathbf{E} \quad (30)$$

$$\mathbf{U} = \mathbf{Q}\mathbf{S}_u\mathbf{E}, \quad (31)$$

where \mathbf{S}_v and \mathbf{S}_u are diagonal matrices having complex numbers of unit magnitude and satisfying the relation of

$$\Delta = \mathbf{S}_u|\Delta|\mathbf{S}_v^H, \quad (32)$$

which means that the phases of the diagonal elements of $\mathbf{S}_u\mathbf{S}_v^H$ should be equal to the diagonal elements of $\Delta/|\Delta|$, the phase components of Δ . Notices that a particular solution of \mathbf{V} when \mathbf{S}_v is the identity matrix becomes $\mathbf{V} = \mathbf{Q}\mathbf{E}$.

Proof: Using the SVD of $\mathbf{H} = \mathbf{U}\Sigma\mathbf{V}^H$, we have

$$\mathbf{H}^H\mathbf{H} = \mathbf{V}\Sigma^2\mathbf{V}^H \quad (33)$$

$$\mathbf{H}\mathbf{H}^H = \mathbf{U}\Sigma^2\mathbf{U}^H. \quad (34)$$

Using the relations of $\mathbf{H} = \mathbf{Q}\Delta\mathbf{Q}^H$ and (32), we get

$$\mathbf{H}^H\mathbf{H} = \mathbf{Q}\Delta^H\Delta\mathbf{Q}^H = \mathbf{Q}\mathbf{S}_v|\Delta|^2\mathbf{S}_v^H\mathbf{Q}^H \quad (35)$$

$$\mathbf{H}\mathbf{H}^H = \mathbf{Q}\Delta\Delta^H\mathbf{Q}^H = \mathbf{Q}\mathbf{S}_u|\Delta|^2\mathbf{S}_u^H\mathbf{Q}^H. \quad (36)$$

Since $|\Delta|^2 = \Delta\Delta^H$, we use (25) and $\tilde{\Delta}^H\tilde{\Delta} = \tilde{\Delta}\tilde{\Delta}^H = \Sigma^2$ to get

$$\begin{aligned} \mathbf{H}^H\mathbf{H} &= \mathbf{Q}\mathbf{S}_v\mathbf{E}\tilde{\Delta}\tilde{\Delta}^H\mathbf{E}^T\mathbf{S}_v^H\mathbf{Q}^H \\ &= \mathbf{Q}\mathbf{S}_v\mathbf{E}\Sigma^2\mathbf{E}^T\mathbf{S}_v^H\mathbf{Q}^H \end{aligned} \quad (37)$$

$$\begin{aligned} \mathbf{H}\mathbf{H}^H &= \mathbf{Q}\mathbf{S}_u\mathbf{E}\tilde{\Delta}\tilde{\Delta}^H\mathbf{E}^T\mathbf{S}_u^H\mathbf{Q}^H \\ &= \mathbf{Q}\mathbf{S}_u\mathbf{E}\Sigma^2\mathbf{E}^T\mathbf{S}_u^H\mathbf{Q}^H \end{aligned} \quad (38)$$

Comparing (33) and (34) with (37) and (38) respectively, we get (30) and (31). \square

Table 1. Feedback parameters and overhead (# of real numbers).

Transmission scheme	Feedback parameters	Feedback overhead
UCA-OAM+EPA	None	0
UCA-MIMO+EPA	None	0
UCA-SVD-MIMO+WF	Mode gains $\{\sigma_k^2\}$	N
UCA-OAM+WF	Mode gains $\{ \delta_i ^2\}$	N

Table 2. Simulation parameters.

Parameter	Value
Carrier frequency	140 GHz
# of UCA elements	8
UCA radius	$R_{TX} = R_{RX} = 25\lambda$
Gain of antenna elements	$\beta = 2$

Table 1 shows the set of parameters required to be fed back from the receiver and the amount of feedback overhead required for precoding and power allocation at the transmitter. In the table, EPA and WF stand for equal power allocation and waterfilling power allocation, respectively.

When the EPA is employed, there is no parameter required to be fed back from the receiver to the transmitter. In the UCA-SVD-MIMO+WF system, however, the singular values should be fed back from the receiver to the transmitter to be used for waterfilling power allocation to achieve the maximum channel capacity [21]. Likewise, the UCA-OAM+WF scheme can achieve the same channel capacity as that of the UCA-SVD-MIMO+WF scheme by feeding back the N mode gains.

IV. NUMERICAL RESULTS AND DISCUSSIONS

In this section, numerical results are presented to verify the validity of the analytical results discussed in section III.

A. Simulation Parameters

Table 2 shows the parameters used in the simulation. In the simulation, the carrier frequency was 140 GHz in the sub-Terahertz band,¹ and both the transmit UCA and the receive UCA were assumed to have eight antenna elements and a radius of 25λ . The gain of each antenna element of the transmit UCA was assumed to be 3 dB (i.e., $\beta = 2$).

The SNR used for the simulation was the SNR that appeared at the receive UCA as defined by (10), and the term ρ needed for the evaluation of the spectral efficiency formula was calculated by (11).

The channel model used in the simulation was the single frequency static channel described in section II-B.

B. Intensity and Phase Fronts of OAM Modes

To verify that the OAM vortex wave can be generated by using a UCA with eight antenna elements, we plotted the intensity fronts and the phase fronts of the OAM modes as shown in Fig. 3 and Fig. 4, assuming that the receive UCA was located at the Rayleigh distance from the transmit UCA. In the figure,

¹Since the Rayleigh distance of a UCA OAM system increases in inverse proportion to the wavelength, the use of RF signals in sub-THz band can achieve the maximum throughput at longer distances compared to the RF signals with lower frequencies.

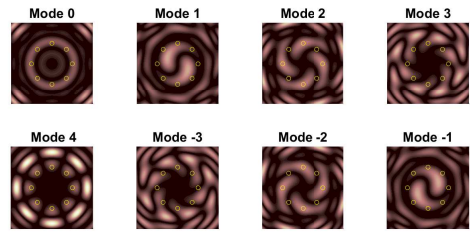


Fig. 3. Intensity fronts of UCA-OAM modes at Rayleigh distance.

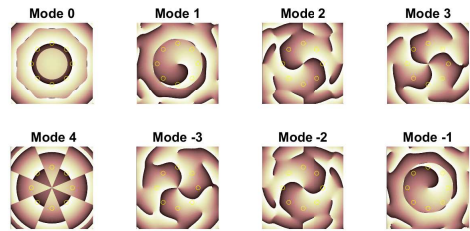


Fig. 4. Phase fronts of UCA-OAM modes at Rayleigh distance.

the intensity and phase fronts denote the intensity and phase of the EM wave appearing at the spots on the plane normal to the beam-axis, and the yellow circles denote the antenna elements of the receive UCA.

In Fig. 3, the six modes except mode 0 and 4 are reminiscent of the vortex waves rotating counter-clockwise or clockwise directions with time, depending on the signs of OAM mode numbers. In addition, Fig. 4 clearly shows the azimuthal phase dependency of the OAM modes observed in the vicinity of the center of the receive UCA, where the phase of the OAM mode l changes linearly from 0 to $2\pi l$.

C. Analysis of Simulation Results

Fig. 5 shows the mode capacity versus T-R distance for the UCA-OAM channel and the UCA-SVD-MIMO channel each having the parameters summarized in Table 2. In the figure, d_R denotes the Rayleigh distance of the LoS UCA-MIMO system at which the columns of the channel matrix become mutually orthogonal. The Rayleigh distance is given by $d_R = \frac{8R_{TX}R_{RX}}{\lambda}$ for $N = 2$, $d_R = \frac{4R_{TX}R_{RX}}{\lambda}$ for $N = 4$ [22] and $d_R = \frac{2R_{TX}R_{RX}}{\lambda}$ for $N = 8$ [8].

The figure reveals that there is a one-to-one correspondence between mode gains of the UCA-OAM channel and eigenvalues of the UCA-SVD-MIMO channel at an arbitrary T-R distance. Taking as an example the T-R distance = 10 m, the channel gains corresponding to the eight OAM modes of the UCA-OAM channel and the eigenvalues corresponding to the eigenmodes of the UCA-SVD-MIMO channel appear as listed in Table 3. This result supports Theorem 2 in Section III that states there exists an eigenmode of the UCA-SVD-MIMO channel with exactly the same eigenvalue as the mode gain of the UCA-OAM channel.

Fig. 6 shows the spectral efficiency that can be obtained with the T-R distance and the SNR when eight data symbol streams are transmitted through the UCA pair channel with the parameters shown in Table 2. In the figure, the simulation results are

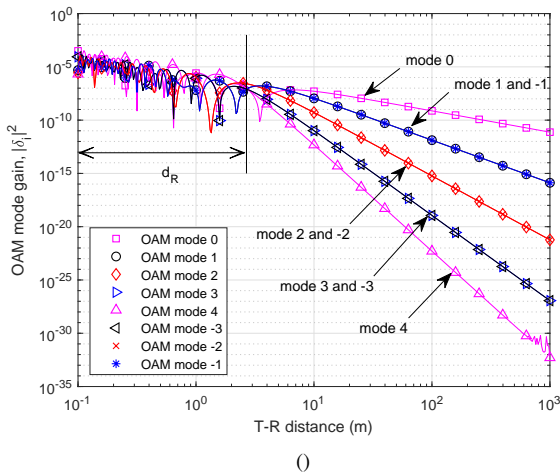
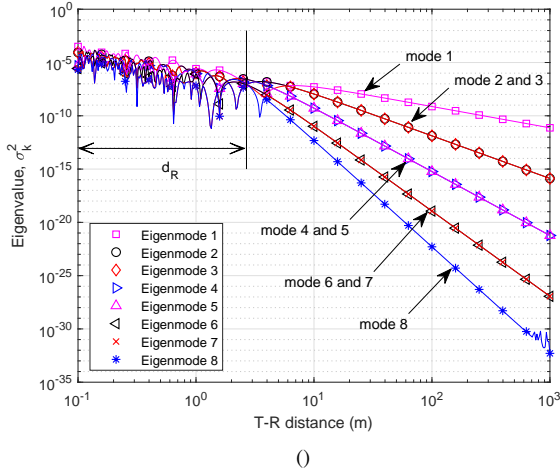


Fig. 5. Mode gains and eigenvalues vs. T-R distance: (a) UCA-OAM and (b) UCA-SVD-MIMO.

Table 3. Mode gains and eigenvalues at T-R distance of 10 m.

UCA-OAM		UCA-SVD-MIMO	
Mode number	Mode gain	Mode number	Eigenvalue
0	5.1361×10^{-8}	1	5.1361×10^{-8}
1	1.1009×10^{-8}	2	1.1009×10^{-8}
2	5.1785×10^{-10}	3	1.1009×10^{-8}
3	1.0306×10^{-11}	4	5.1785×10^{-10}
4	4.7278×10^{-13}	5	5.1785×10^{-10}
-3	1.0306×10^{-11}	6	1.0306×10^{-11}
-2	5.1785×10^{-10}	7	1.0306×10^{-11}
-1	1.1009×10^{-8}	8	4.7278×10^{-13}

shown for the following four cases.

1. UCA-OAM+WF : When the waterfilling power allocation is applied to the UCA-OAM transmission scheme.
2. UCA-SVD-MIMO+WF : When the waterfilling power allocation is applied to the UCA-SVD-MIMO scheme.
3. UCA-OAM+EPA : When the equal power allocation is applied to the UCA-OAM scheme.
4. UCA-MIMO+EPA : When the equal power allocation is applied to the open-loop MIMO scheme.

In the figure, in the near-field zone with a T-R distance shorter than the Rayleigh distance, all four cases show the same spectral

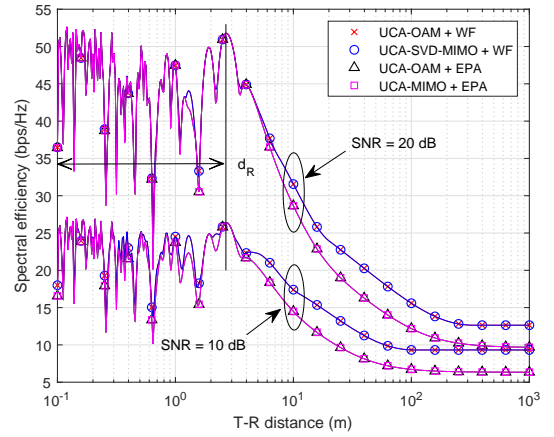


Fig. 6. Spectral efficiency vs. T-R distance.

Table 4. Spectral efficiency at the T-R distance of 10 m.

SNR	UCA-OAM+EPA	UCA-OAM+WF	Improvement
10 dB	14.48 bps/Hz	17.41 bps/Hz	20.17%
20 dB	28.65 bps/Hz	31.56 bps/Hz	10.16%

efficiency regardless of whether or not the waterfilling power allocation is employed. Moreover, in the far-field zone of a T-R distance greater than the Rayleigh distance, there is an improvement in the spectral efficiency due to the application of the waterfilling power allocation. In addition, the spectral efficiency in the near-field zone does not decrease monotonically with the T-R distance and shows a large fluctuation.

In the far-field zone where the T-R distance is greater than the Rayleigh distance, the UCA-OAM+EPA and UCA-MIMO+EPA schemes employing the equal power allocation show the same spectral efficiency in both cases where $SNR = 10$ dB and $SNR = 20$ dB, which coincides with the analytical result in Section III-A.

In addition, as analyzed in Section III-C, the UCA-OAM+WF scheme with the waterfilling power allocation shows the same spectral efficiency as that of the UCA-SVD-MIMO+WF scheme.

Comparing the graphs for the UCA-OAM+WF and UCA-OAM+EPA in the figure, it is also found that the UCA-OAM+WF scheme has greater spectral efficiency than the UCA-OAM+EPA with additional feedback overhead of just N real numbers. For example, when the T-R distance is 10 m, as shown in Table 4, the UCA-OAM+WF scheme shows an increase in spectral efficiency of 20.17% and 10.16% compared to the UCA-OAM+EPA scheme at $SNR = 10$ dB and $SNR = 20$ dB, respectively.

D. On the Error Rate Performance

In order to compare the error rate performances of the above 4 transmission schemes, a simulation on the symbol error rate (SER) performance was conducted for the SNRs of 10 dB and 20 dB. In the simulation, it was assumed that all 8 streams were QPSK encoded and the zero-forcing V-BLAST algorithm was applied for the detection of the multiplex streams. For the decoding of QPSK symbols, the maximum likelihood decoding

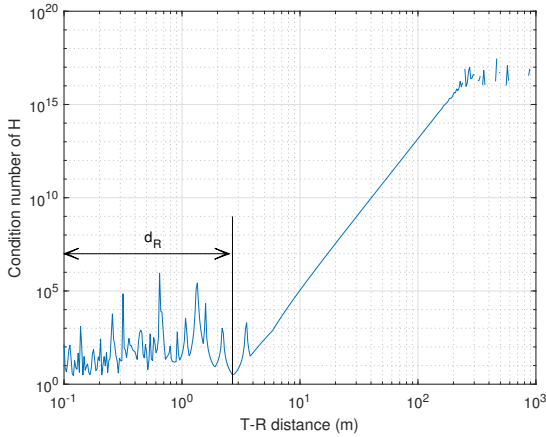


Fig. 7. Condition number of UCA pair channels.

rule was applied for each stream.

Fig. 7 shows the variation of the condition number of the UCA pair channel with the T-R distance, where it can be seen that the condition number becomes the minimum at the Rayleigh distance. Fig. 8 shows that all four transmission schemes have the same lowest SER at the Rayleigh distance, and it also shows that both the UCA-OAM system and the UCA-SVD-MIMO system experience the same level of SER under the equal power allocation. In addition, it shows that the SER increases rapidly as the T-R distance increases beyond the Rayleigh distance. This is caused by the large condition number of the UCA pair channel at such T-R distance, in which case the aggregated SER becomes large because the streams assigned to those modes with relatively low eigenvalues experience high SERs.

There is one peculiarity observed in Fig. 8. In T-R distances around Rayleigh distance, the transmission schemes with waterfilling power allocation is observed to have a higher SER than the schemes with equal power allocation. This is a direct contradiction to the expectation that a system with waterfilling power allocation will have a lower SER than a system with equal power allocation. The reason why this happened is because the same modulation level was applied for all the streams even for the schemes with waterfilling power allocation without regarding the allocated powers for them. This indicates that, in order to realize an improved spectral efficiency by adopting waterfilling power allocation, it is necessary to apply modulation levels and code rates appropriate for the streams regarding the allocated powers.

V. CONCLUSION

In this paper, the UCA-OAM scheme over the UCA-SVD-MIMO scheme have been compared in terms of spectral efficiency and feedback overhead.

As a result of the analysis, it was found that the UCA-OAM scheme achieves the same spectral efficiency as the UCA-SVD-MIMO scheme with the exactly same feedback overhead.

In addition, it was found that the UCA-OAM+WF scheme can improve the spectral efficiency compared to the UCA-OAM scheme at the expense of an additional feedback overhead of the

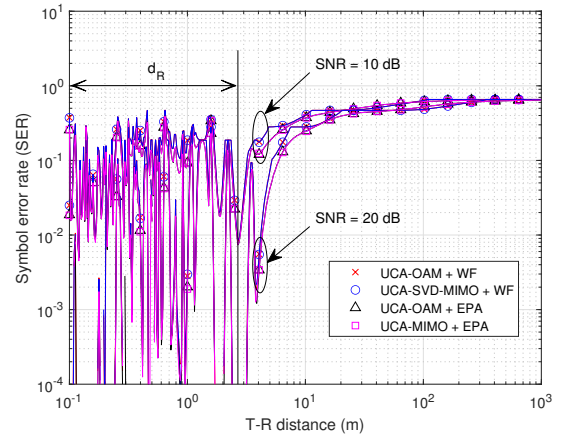


Fig. 8. Comparison of symbol error rates.

OAM mode gains.

REFERENCES

- [1] J. D. Jackson, "Classical Electrodynamics," Wiley, New York, 1962.
- [2] A. E. Willner *et al.*, "Optical communications using orbital angular momentum beams," *Advances Optics Photonics*, vol. 7, no. 1, pp. 66–106, Mar. 2015.
- [3] J. Wang *et al.*, "Terabit free-space data transmission employing orbital angular momentum multiplexing," *Nature Photon.*, vol. 6, pp. 488–496, July 2012.
- [4] L. Wang, X. Ge, R. Zi, and C.-X. Wang, "Capacity analysis of orbital angular momentum wireless channels," *IEEE Access*, vol. 5, pp. 23069–23077, Oct. 2017.
- [5] F. Tamburini *et al.*, "Encoding many channels on the same frequency through radio vorticity: First experimental test," *New J. Physics*, vol. 14, no. 3, pp. 1–16, Mar. 2012.
- [6] B. Thidé *et al.*, "Utilization of photon orbital angular momentum in the low-frequency radio domain," *Phys. Rev. Lett.*, vol. 99, no. 8, pp. 087701-1–087701-4, Aug. 2007.
- [7] S. M. Mohammadi *et al.*, "Orbital angular momentum in radio - A system study," *IEEE Trans. Antennas Propag.*, vol. 58, no. 2, pp. 565–572, Feb. 2010.
- [8] O. Edfors and A. J. Johansson, "Is orbital angular momentum (OAM) based radio communication an unexploited area?," *IEEE Trans. Antennas Propag.*, vol. 60, no. 2, pp. 1126–1131, Feb. 2012.
- [9] X. Ge, R. Zi, X. Xiong, Q. Li, and L. Wang, "Millimeter wave communications with OAM-SM scheme for future mobile networks," *IEEE J. Sel. Areas Commun.*, vol. 35, no. 9, pp.2163–2177, Sept. 2017.
- [10] Y. Yan *et al.*, "High-capacity millimetre-wave communications with orbital angular momentum multiplexing," *Nature Commun.*, vol. 5, no. 4876, pp. 1–9, Sept. 2014.
- [11] Y. Ren *et al.*, "Line-of-sight millimeter-wave communications using orbital angular momentum multiplexing combined with conventional spatial multiplexing," *IEEE Trans. Wireless Commun.* vol. 16, no. 5, pp. 3151–3161, May 2017.
- [12] R. Gaffoglio, A. Cagliero, G. Vecchi, and F. P. Andriulli, "Vortex waves and channel capacity: hopes and reality," *IEEE Access*, vol. 6, pp. 19814–19822, Dec. 2017.
- [13] R. Chen, H. Xu, M. Moretti, and J. Li, "Beam steering for the misalignment in UCA-based OAM communication system," *IEEE Wireless Commun. Lett.*, vol. 7, no. 4, pp. 582–585, Aug. 2018.
- [14] R. Chen, H. Zhou, M. Moretti, X. Wang, and J. Li, "Orbital angular momentum waves: Generation, detection and emerging applications," *IEEE Commun. Surveys Tuts.*, vol. 22, no. 2, pp. 840–868, Secondquarter 2020.
- [15] G. Molina-Terriza, J. P. Torres, and L. Torner, "Management of the angular momentum of light: propagation of photons in multi-dimensional vector states of angular momentum," *Phys. Rev. Lett.*, vol. 88, pp. 013601, 2002.
- [16] J. Ren, K. W. Leung, "Generation of microwave orbital angular momentum states using hemispherical dielectric resonator antenna," *Appl. Physics Lett.*, vol. 112, no. 13, Mar. 2018.
- [17] W. Zhang *et al.*, "Four-OAM-mode antenna with traveling-wave ring-

slot structure," *IEEE Antennas Wireless Propagation Lett.*, vol. 16, pp. 194–197, 2017.

- [18] S. Yu *et al.*, "Design, fabrication, and measurement of reflective metasurface for orbital angular momentum vortex wave in radio frequency domain," *Appl. Physics Lett.*, vol. 108, no. 12, Mar. 2016.
- [19] X. Meng *et al.*, "Generation of multiple beams carrying different orbital angular momentum modes based on anisotropic holographic metasurfaces in the radio-frequency domain," *Appl. Physics Lett.*, vol. 114, no. 9, Mar. 2019.
- [20] K. Zhang *et al.*, "High efficiency metalenses with switchable functionalities in microwave region," *Appl. Materials Interfaces*, vol. 11, no. 31, pp. 28423–28430, July 2019.
- [21] A. Goldsmith, S. A. Jafar, N. Jindal, and S. Vishwanath, "Capacity limits of MIMO channels," *IEEE J. Sel. Areas Commun.*, vol. 21, no. 5, pp. 684–701, June 2003.
- [22] F. Bohagen, P. Orten, and G. E. Oien, "Optimal design of uniform planar antenna arrays for strong line-of-sight MIMO channels," *EURASIP J. Wireless Commun. Netw.*, vol. 2007, no. 1, pp. 1–10, 2007.



Gye-Tae Gil received the B.S. degree in Electronic Communication Engineering from Hanyang University, Seoul, South Korea, in 1989, and the M.S. and Ph.D. degrees in Electrical Engineering from the Korea Advanced Institute of Science and Technology (KAIST), South Korea, in 1992 and 2004, respectively. Since 1991, he has been with the Research Center of Korea Telecom, and joined the KAIST Institute in 2013, where he is currently a Research Professor. His research interests are in the area of communication signal processing, which includes synchronization,

interference cancellation, and adaptive filter design. He is also interested in orbital angular momentum transmission and massive antenna technologies for cellular mobile communication systems.



Ju Yong Lee received the B.S., M.S., and Ph.D. degrees in Electrical Engineering and Computer Science from the Korea Advanced Institute of Science and Technology (KAIST), Daejeon, Korea, in 1995, 1997, and 2003, respectively. He was a Senior Researcher with the System R&D team, Network Systems Division, Samsung Electronics, from 2003 to 2006. He was also a Postdoctoral Fellow with the University of Toronto, Toronto, ON, Canada, from 2007 to 2008. He was a Research Professor with Sungkyunkwan University, Korea, in 2009. He is currently a Team Leader

and Research Professor with the communication and energy team, KAIST Institute for Information Technology Convergence. His current research interests include future wireless communication networks and wireless power transfer technology.



Optics Express.

Hoon Kim is an Associate Professor of the School of Electrical Engineering at KAIST. Prior to joining KAIST in 2014, he was with Bell Labs, Lucent Technologies (2000–2001), Samsung Electronics, Korea (2001–2007), and National University of Singapore (2007–2014). His research interests include high-capacity fiber-optic communication systems, free-space optical communications, fiber-optic mobile fronthaul/backhaul systems, and lightweight subsystems. He serves as a Senior Editor of *IEEE Photonics Technology Letters* and an Associate Editor of



to 2015. He was also an IT Convergence Campus (ICC) Vice-President of KAIST from 2011 to 2013. His research interests include mobile communication, online electric vehicle system based on wireless power transfer, and bioinformatics.

Dong-Ho Cho received the Ph.D. degree in Electrical Engineering from KAIST in 1985. From 1987 to 1997, he was a Professor with the Department of Computer Engineering, Kyunghee University. Since 1998, he has been a Professor with the School of Electrical Engineering, KAIST. He was a Director of the Institute for Information Technology Convergence, KAIST, from 2007 to 2011. He has been the Director of the KAIST Online Electric Vehicle Project since 2009. He was the Head of The Cho Chun Shik Graduate School for Green Transportation from 2010